Electrochemical Materials and Technologies

ARTICLE

Structural stability and features of electrical and electrochemical behavior under reducing conditions of $Pr_{0.4}Sr_{0.6}Co_{0.2}Fe_{0.7}Nb_{0.1}O_{3-\delta}$ material for the symmetrical SOFCs

Elena Pikalova [a], Denis Osinkin [a, *]

In this study, a performance of the complex oxide composition of $Pr_{0.4}Sr_{0.6}Co_{0.2}Fe_{0.7}Nb_{0.1}O_{3-\delta}$ was investigated from the viewpoint of its use as a fuel or symmetrical electrode for the electrochemical devices with a $LaGaO_3$-based solid electrolyte. The results show that the above-mentioned oxide can be obtained as a single-phase composition using solid-phase synthesis with a final annealing temperature of 1150 °C. It has been shown that the oxide retains satisfactory stability at 800 °C in an atmosphere of 5 % H_2 + Ar, only a minor amount, presumably of Co-Fe alloy, has been detected. The electrical conductivity of the oxide in wet hydrogen exhibits a linear semiconductor-type behavior with a conductivity value of 7 S · cm^{-1} at 800 °C. The polarization resistance of the $Pr_{0.4}Sr_{0.6}Co_{0.2}Fe_{0.7}Nb_{0.1}O_{3-\delta}$ electrode in wet hydrogen atmosphere reaches approximately 1.09 Ω · cm^2 at 800 °C, which is a relatively high value for the electrodes of electrochemical devices. A significant reduction in resistance down to 0.43 Ω · cm^2 is observed for the electrode activated with impregnated ceria. It has been demonstrated that the observed decrease in resistance is due to the expansion of the area of the electrochemical reaction without changing its mechanism. The long-term tests with a duration of about 220 h at 800 °C in a wet hydrogen atmosphere demonstrate satisfactory stability of the electrochemical activity of the $Pr_{0.4}Sr_{0.6}Co_{0.2}Fe_{0.7}Nb_{0.1}O_{3-\delta}$ electrode, which can be considered as a promising electrode for intermediate temperature electrochemical devices, including those of symmetrical design.

1. Introduction

Solid oxide fuel cells (SOFCs) offer high efficiency in the direct conversion of chemical energy to electricity and fuel flexibility due to their ability to operate at higher temperatures than other types of fuel cells [1, 2]. Modern SOFC research has focused on decreasing the operating temperature to the intermediate range (600–750 °C) [3, 4]. The primary objective was to promote the use of low-cost electrode materials, and decrease material demands for seals and balance-of-plant components [5–7].

This could help to significantly reduce the cost of the cells and facilitate their commercialization [8]. Furthermore, a cell operating at a decreased temperature would allow for a quicker start and an improvement in cell durability due to lower degradation of the materials comprising the SOFC. Unfortunately, decreasing the operation temperature causes the rapid increase in the ohmic resistance of the electrolyte and polarization resistance for traditional electrode materials (especially the cathode materials) because of the high activation energy of oxygen reduction [3, 9, 10]. The problem with high resistivity of electrolyte membranes can be partly resolved by decreasing the membrane thickness via transition to the use of the electrode or metal-supported constructions of SOFCs [11–13] or by means of the development of new electrolyte materials with higher conductivity in the IT-range compared to that of Y_2O_3-stabilized ZrO_2,

a: Kinetics laboratory, Institute of high-temperature electrochemistry, Yekaterinburg 620066, Russia

* Corresponding author: OsinkinDA@mail.ru

traditionally used in high-temperature electrochemical devices [14–16]. Therefore, exploring new electrode materials with high conductivity and catalytic activity by optimizing both the structural and elemental compositions to achieve low polarization resistance is a critical issue for the SOFCs, operating in the intermediate temperature range (IT-SOFCs).

Favorable electrode materials for IT-SOFC require substantially high mixed ionic and electronic conductivity (MIEC). As for example, using MIEC materials as a SOFC cathode the possibility to extend the effective zone for oxygen reduction reaction (ORR) to the whole surface of the electrode, thus ensuring preservation of high electrochemical activity in the IT-range. Oxide materials, possessing the perovskite structure, particularly of the ABO_3 type, where with A-site element such as Lanthanide (La, Pr, Nd, Sm, Gd, etc.), Strontium (Sr) or Barium (Ba) and the B-site element such as Mn, Fe, Cu, Ni, Co are used as cathodes in SOFCs operating in a wide range of temperature regimes [17–19]. Among them, $La_{1-x}Sr_xCoO_{3-\delta}$ (LSC), $La_{1-x}Sr_xCo_{1-y}Fe_yO_{3-\delta}$ (LSCF) and $Ba_{0.6}Sr_{0.4}Co_{0.2}Fe_{0.8}O_{3-\delta}$ (BSCF) are the most studied and commercially available owing to the remarkable electronic conductivity, excellent ionic migration, favorable catalytic activity. However, such drawback of these materials as low phase stability (BSCF [20]), Sr-segregation during long-term operation (all of the above [21–23]), poor chemical and thermomechanical compatibility with widely used ZrO_2 and $LaGaO_3$-based materials and proton-conducting electrolytes (all of the above [24, 25]) facilitated the search for new SOFC cathodes [26–29].

The catalytic properties of the anode to the fuel oxidation reaction are also important, particularly as the operating temperature decreases [30–33]. In recent decades, the composites of metallic nickel and a ceramic component based on doped zirconia or ceria have been considered as the main material for SOFC anodes due to their high conductivity and catalytic activity in the hydrogen oxidation reaction, as well as their moderate cost [34]. The following aspects can be identified as disadvantages of using Ni-cermets: agglomeration of metallic nickel particles during long-term operation at high temperatures, which results in a reduction in conductivity level [35], deposition of carbon on the surface and sulfur poisoning when using hydrocarbons as a fuel [36], mechanical instability during redox cycling, associated with a significant difference in the density of Ni and NiO. There is currently no complete solution to all of the above problems. Perovskite-based anodes also could be the promising candidates for IT-SOFCs, especially

fueled with various hydrocarbon fuels, due to their high redox stability, satisfactory electric and/or ionic conductivity, high activity towards fuel decomposition and better resistance towards carbon deposition and sulfur poisoning compared to the traditionally used Ni-cermets [33]. It would be also favorable to find materials successfully operating both as an air and a fuel electrode [37, 38].

In addition to the aforementioned drawbacks of MIEC electrodes, it is also important to note that the majority of MIEC electrodes are prone to intrinsic degradation. This is mainly due to the instability of the perovskite structure and the depletion of alkali earth elements present in the structure, particularly when exposed to carbon-containing atmospheres [22, 39, 40]. It was shown, that the stability of the perovskites can be improved by introducing high valence metal ions [41]. It is noteworthy that this strategy can be employed to enhance the stability of both anode and cathode materials [42–47].

Recently, $Pr_{1-x}Sr_xCo_yFe_{1-y}O_{3-\delta}$ (PSCF) and its derivatives have attracted significant interest as prospective materials for cathodes [48–51], anodes [52], both cathode and anode in symmetrical cells [53, 54], for reversible and single-component cells [55], as well as oxygen permeation membranes [56, 57]. Ishihara et al. [58], studying $Ln_{0.6}Sr_{0.4}MnO_3$ (Ln = La, Pr, Nd, Sm, Gd, Yb, Y), demonstrated that Pr-based perovskite showed the highest electrical conductivity and the lowest overpotential value as a consequence of Pr^{3+}/Pr^{4+} valence change. The strategy to improving the PSCF stability and functional properties by means of doping with high valence metal ions on the B-site was also considered in a number of studies.

Zhang et al. [59] explored the potential of Mo-doped $Pr_{0.4}Sr_{0.6}Co_{0.2}Fe_{0.8}O_{3-\delta}$ (PSCFM) as a cathode material. Their findings indicated that Mo doping resulted in a slight reduction in electrical conductivity, attributed to the formation of additional oxygen vacancies. It allowed decreasing the Mo-doped PSCF cathode polarization resistance down to 0.22, 0.06 and 0.025 $\Omega \cdot cm^2$ at 600, 700 and 800 °C, respectively, used in contact with the LSGM electrolyte, highly promising for IT-SOFC [16, 60]. These values were much lower than those reported for the composite electrodes based on PSCF such as $Pr_{0.6}Sr_{0.4}Co_{0.8}Fe_{0.2}O_{3-\delta} - Ce_{0.85}Gd_{0.15}O_{1.925}$ (50 : 50) on the $Ce_{0.85}Gd_{0.15}O_{1.925}$ electrolyte (0.046 $\Omega \cdot cm^2$ at 800 °C [48]) and $Pr_{0.6}Sr_{0.4}Co_{0.8}Fe_{0.2}O_{3-\delta} - Ce_{0.9}Gd_{0.1}O_{1.9}$ (CGO) (50 : 50) on the 8YSZ electrolyte with the CGO barrier layers (0.12 $\Omega \cdot cm^2$ at 800 °C [49]). In [59], the fabricated single cell with the 275 µm thick LSGM electrolyte membrane, the Mo-doped PSCF cathode and

the NiO – SDC anode exhibited the peak power densities of 0.319, 0.442 and 0.555 W $\cdot$ cm^{-2} at 700, 750 and 800 °C, respectively. The 100-hour stability test result for this cell under a constant current load of 0.44 A $\cdot$ cm^{-2} at 700 °C demonstrated only a slight decrease of the output voltage during the first 5 h, and then a relatively stable performance was observed from 5 to 100 h. The same authors [53] considered $(Pr_{0.4})_xSr_{0.6}Co_{0.2}Fe_{0.7}Nb_{0.1}O_{3-\delta}$ ($0.9 \leq x \leq 1.1$) to solve the carbon deposition and sulfur adsorption problems during the operation of the symmetrical SOFC with LSGM electrolyte. The polarization resistance of the $P_{1.05}SCFN$ electrode was the lowest in the series and amounted 0.012 and 0.15 $\Omega \cdot$ cm^2 at 850 °C in wet air and H$_2$, respectively. The obtained maximum power densities of the $P_{1.05}SCFN/LSGM/P_{1.05}SCFN$ cell were as high as 1.13 W $\cdot$ cm^{-2} in wet H$_2$ and 0.67 W $\cdot$ cm^{-2} in wet CH$_4$ at 900 °C. Unfortunately, the authors did not provide the stability tests.

In the study of Li et al. [55], $Pr_{0.4}Sr_{0.6}Co_{0.2}Fe_{0.7}Nb_{0.1}O_{3-\delta}$ was found to exhibit high catalytic activity for both oxygen reduction and hydrogen oxidation reactions. For the reversible single-component cell with $Sm_{0.2}Ce_{0.8}O_2$ (SDC) – $(Li/Na)_2CO_3$ fueled with 53 % H$_2$ – 47 % H$_2$O, the peak power densities were 0.180, 0.143, and 0.106 W $\cdot$ cm^{-2} the SOFC mode, while the current densities were 0.265, 0.206, and 0.127 A $\cdot$ cm^{-2} under 1.3 V in the SOEC mode at 700, 650, and 600 °C, respectively. Following three cycles of operation, lasting four hours each, the cell performance exhibited a decline in the SOFC mode and an improvement in the SOEC mode.

Xiaokaiti et al. [54] showed that in the $Pr_{0.4}Sr_{0.6}Co_{0.9-x}Fe_xNb_{0.1}O_{3-\delta}$ ($x = 0$, 0.2, 0.4, 0.6 and 0.9) series, the material with medium Fe content ($x = 0.6$, PSCF$_{0.6}$N) exhibited the lowest polarization resistance equal to 0.028 and 0.077 $\Omega \cdot$ cm^2 (at 900 °C, in air and hydrogen, respectively) and the highest electrical conductivity of 258.9 S $\cdot$ cm^{-1} (at 650 °C). Fe-doping decreased the thermal expansion coefficient (TEC) value from 17.39 (PSCN) down to 11.79 $\cdot$ 10^{-6} K^{-1} (PSCF$_{0.6}$N), which improved the thermomechanical compatibility with the LSGM electrolyte. The single electrolyte-supported symmetrical SOFCs with different electrolyte thicknesses of 500, 400 and 300 μm showed the power peak densities 0.642, 0.713 and 0.891 W $\cdot$ cm^{-2}, respectively.

In this study, the material with moderate Fe-doping of $Pr_{0.4}Sr_{0.6}Co_{0.2}Fe_{0.7}Nb_{0.1}O_{3-\delta}$ (PSCFN) was selected based on the available literature data to investigate its potential as a fuel electrode material for the IT-SOFCs based on the LSGM electrolyte. Given that the majority of the studies

of the electrodes for symmetrical SOFCs demonstrated higher polarization resistance in hydrogen compared to that in air, consequently this study was directed towards investigating phenomena in the PSCFN electrode in hydrogen with the aim of determining their impact on the electrode performance. The study was conducted using electrochemical impedance spectroscopy (EIS) method in conjunction with the comprehensive spectra analysis via the distribution of relaxation times (DRT) method. Moreover, the influence of the activation and the long-term stability of the electrode characteristics in hydrogen were investigated as important indicators for the electrode practical application.

2. Experimental

$Pr_{0.4}Sr_{0.6}Co_{0.2}Fe_{0.7}Nb_{0.1}O_{3-\delta}$ (PSCFN) perovskite was prepared by the three-step solid-state reaction method from the $Pr(NO_3)_3 \cdot 6H_2O$ (99.9 %), $SrCO_3$ (99.999 %), $Co(NO_3)_2 \cdot 6H_2O$ (99.9 %), Fe_2O_3 (98.7 %) and Nb_2O_5 (99.9 %) initial reagents. The stoichiometric amounts of these materials were mixed with ethanol in a planetary ball mill Retsch PM 100 for 1 h. The resulting mixture was dried at 100 °C for 12 h and stepwise calcined in air for 10 h at 1050 °C and 10 h at 1150 °C with the intermediate mechanical activation by means of the ball-milling for 1 h. The XRD analysis of the PSCFN samples after synthesis and after temperature treatment at 800 °C in the 5 vol. % H$_2$ + Ar gas mixture was carried out using a Rigaku D/MAX-2200VIPC diffractometer.

Synthesis of the $La_{0.85}Sr_{0.15}Ga_{0.85}Mg_{0.15}O_{3-\delta}$ (LSGM) electrolyte was performed from the oxide and carbonate powders of La_2O_3 (99.99 %), Ga_2O_3 (99.999 %), $SrCO_3$ (99.99 %), $(MgCO_3)_4 \cdot Mg(OH)_2 \cdot 5H_2O$ (99.99 %) as described elsewhere [61]. The calcination temperature of the electrolyte powder was 1200 °C 1 h. Then, the powder was pressed under isostatic conditions at 625 MPa into disk-shape substrates and sintered for 10 h at 1450 °C. After sintering, the prepared samples consisted of pure LSGM perovskite phase with a unit cell parameter equal to 3.91377(8) Å. The relative density of the electrolyte substrates defined after their polishing using a diamond disk was approximately 97 % of the theoretical one.

The conductivity the compact bar-shaped PSCFN sample sintered at 1250 °C for 4 h (relative density of 95 %) was measured using the 4-probe dc current method in a wet hydrogen. For electrochemical studies the electrode slurry was prepared by mixing the PSCFN powder with polyvinyl butyral binder and isopropyl alcohol. The slurry was applied to both sides of the LSGM electrolyte substrate. After sintering at 1250 °C for 2 h in air, the electrode area and thickness were about 0.3 cm^2

and 19 μm, respectively. The electrochemical studies were performed by means of the impedance spectroscopy in the frequency range of 10^4–10^{-2} Hz using an FRA-1260 and EI-1287 electrochemical interface. A Pt mesh and wires were used as a current collector. The high-temperature studies were performed in wet hydrogen at the atmospheric pressure. To investigate the influence of the electrode activation on its performance, the electrode was impregnated with the $Ce(NO_3)_3$ solution as described elsewhere [62] followed by thermolysis in wet hydrogen. To identify the features of the electrode reactions without and with impregnation, the distribution of relaxation time (DRT) analysis was performed using a program code based on Tikhonov's regularization [63].

3. Results and discussion

3.1. Structure features in oxidizing and reducing atmospheres

The XRD pattern of the PSCFN powder obtained after synthesis and after high-temperature treatment under reducing conditions are represented in Figure 1. The peak positions of PSCFN were consistent with those of the standard card ($Pr_{0.5}Sr_{0.5}$)FeO_3 (PDF#75–4528), indicating that the PSCFN crystallized in the orthorhombic *Pnma* (62) space group with the unit cell parameters of $a = 5.4893(21)$ Å, $b = 7.7638(88)$ Å and $c = 5.4911(34)$ Å. After the treatment in the 5 vol. % H_2 + Ar gas mixture at 800 °C, on the X-ray diagram there is a peak of low intensity in the region of angles 45 ° apparently from the Co-Fe alloy. Yang et al. [52] also revealed the orthorhombic structure for the PSCFN material obtained by a solid-state reaction method in air.
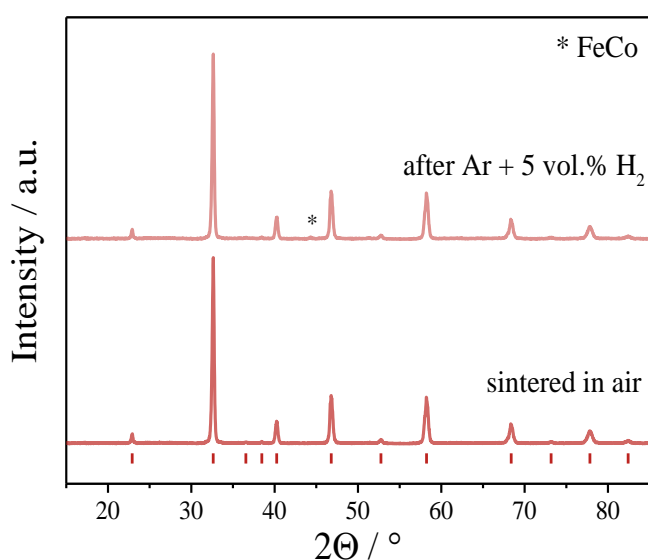
Figure 1 XRD patterns of the PSCFN powder obtained after synthesis and after treatment at 800 °C in the 5 vol. % H_2 + Ar mixture and Bragg's positions.

The authors observed the transformation of orthorhombic PSCFN to K_2NiF_4-type structured $Pr_{0.8}Sr_{1.2}(Co,Fe)_{0.8}Nb_{0.2}O_{4+\delta}$ with homogeneously dispersed nano-sized Co-Fe alloy after the treatment in H_2 at 900 °C. This transition was found to be reversible. Zhang et al. [53] demonstrated that single-phase materials in the $(Pr_{0.4})_xSr_{0.6}Co_{0.2}Fe_{0.7}Nb_{0.1}O_{3-\delta}$ series, obtained by the solid-state reaction method, possessed a cubic structure across the *A*-site nonstoichiometry range of $x = 0.9$–1.05. It is important to note that the $Pr_{0.4}Sr_{0.6}Co_{0.3}Fe_{0.6}Nb_{0.1}O_{3-\delta}$ material with a composition similar to that considered in this study was shown to have a cubic structure of *Pm-3m* (221) space group. The specific feature of the material was that it transformed reversibly to a tetragonal *I4/m* (87) phase following hydrogen treatment at 1000 °C for 3 h [54].

3.2. Conductivity data

According to the data presented in literature, materials of the $Pr_{0.4}Sr_{0.6}(Co_{0.3}Fe_{0.6})_{1-x}Nb_xO_{3-\delta}$ series demonstrate in the oxidizing atmospheres an extremal dependence of the conductivity on temperature. They display a thermally activated behavior at lower temperature where the conductivity increases with the temperature growth up to a transition temperature in the range of 500–600 °C, which shifted to lower temperature with increasing the Nb content [64]. With further increasing the temperature over the transition point (T_{max}), the conductivity decreases, which can be caused by the loss of oxygen from the perovskite structure with the oxygen vacancies formation. This phenomenon known as pseudo-metallic behavior was determined by Patrakeev et al. to be offset by a reduction in charge carrier concentration, resulting in an overall reduction in electronic conductivity with increasing temperature [65].

The Nb doping results in a decrease in conductivity due to reduction of Fe^{4+} and Co^{4+} to Fe^{3+} and Co^{3+} to maintain the charge balance (Table 1). Despite the reduction in the total conductivity, the Nb doping is supposed to recover the transport chains for holes and improve their mobility as a result of increasing the lattice free volume (the ionic radius of Nb^{5+} (67 pm) is significantly larger than Fe^{4+} (58.5 pm) as well as Co^{4+} (53 pm) [66]) and a decrease in the metal-oxygen average bond energy. Moreover, Fe and Co reduction in the Nb-doped material results in increasing the oxygen vacancies content on the material's surface, which was approved by the XPS study in [64] and, therefore, may enhance the catalytic activity of the material towards electrode reactions due to increasing the rate of oxygen exchange. As shown in Table 1, a little amount of Nb doping ($x = 0.05$) results in the increase in activation energy,

indicating a decrease in the activity. However, with the further increasing the Nb doping content the catalytic activity increased. For Mo-doped materials, the $E_{a_{ox}}$ minimum was observed at $x = 0.05$ [67]. When moving into atmospheres with a reduced partial pressure of oxygen (air → Ar → Ar + 5 vol. % H_2), the conductivity decreases and severity of the maximum on the curves of the dependence of conductivity on temperature naturally becomes smoother [53], turning into approximately linear dependence in wet H_2 in the temperature range of 550−900 °C, which was demonstrated in this work (Figure 2). The values of conductivity obtained for PSCFN in reducing atmospheres usually do not exceed $10 \ S \cdot cm^{-1}$, which agrees well with those for other oxide anode materials (Table 1), except for the materials that demonstrated higher conductivity due to the presence of exsolved Fe [68] and Fe-Ni alloy [69] particles.
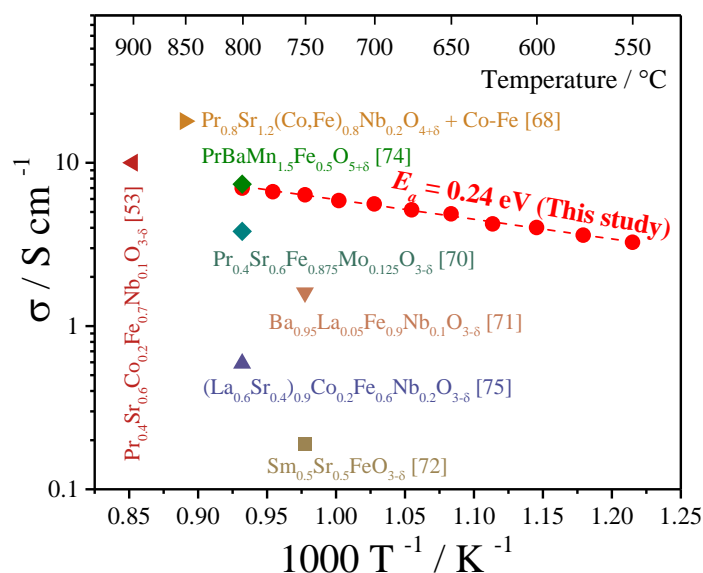
Figure 2 Electrical conductivity of PSCFN obtained in this study (shown by red color) and other oxides under reduction condition.

Table 1 – Conductivity of the electrode materials promising for the symmetrical SOFC application ion oxidizing (σ_{ox}) and reducing (σ_{red}) atmospheres ("−" shows that there were no data available).

Electrode material	T, °C	σ_{ox}, $S \cdot cm^{-1}$	$E_{a_{ox}}$, eV (T range, °C)	σ_{red}, $S \cdot cm^{-1}$	$E_{a_{red}}$, eV (T range, °C)	Ref.
$Pr_{0.4}Sr_{0.6}(Co0.3Fe_{0.6})_{1-x}Nb_xO_{3-\delta}$ ($x = 0.05, 0.1, 0.2$)	800	170 110 70	0.117 0.107 0.104 ($100-T_{max}$)	–	–	[64]
$Pr_{0.4}Sr_{0.6}Co_{0.2}Fe_{0.75}Mo_{0.05}O_{3-\sigma}$ $Pr_{0.4}Sr_{0.6}Co_{0.2}Fe_{0.7}Mo_{0.1}O_{3-\sigma}$ $Pr_{0.4}Sr_{0.6}Co_{0.2}Fe_{0.6}Mo_{0.2}O_{3-\sigma}$	900	105 70 40	0.093 0.123 0.157 ($200-T_{max}$)	–	–	[67]
$Pr_{0.8}Sr_{1.2}(Co,Fe)_{0.8}Nb_{0.2}O_{4+\delta}$ + + Co-Fe alloy ($Pr_{0.4}Sr_{0.6}Co_{0.2}Fe_{0.7}Nb_{0.1}O_{3-\sigma}$ reduced in H_2 at 900 °C)	850	–	–	18 (H_2)	–	[68]
$Pr_{0.4}Sr_{0.6}Co_{0.2}Fe_{0.7}Nb_{0.1}O_{3-\sigma}$	900	107	–	25 (Ar) 10 (Ar + H_2)	–	[53]
$Pr_{0.4}Sr_{0.6}Co_{0.2}Fe_{0.7}Nb_{0.1}O_{3-\delta}$	800 700 600	–	–	7.0 (wet H_2) 5.6 (wet H_2) 3.9 (wet H_2)	0.24 (300−900)	This study
$Pr_{0.4}Sr_{0.6}Fe_{0.875}Mo_{0.125}O_{3-\delta}$	800	71	–	3.8 (wet H_2)	–	[70]
$Ba_{0.95}La_{0.05}Fe_{0.9}Nb_{0.1}O_{3-\delta}$	750	5	–	1.6	–	[71]
$Sm_{0.5}Sr_{0.5}FeO_{3-\delta}$	750	160	–	0.19 (H_2)	–	[72]
$SrFe_{0.8}Cu_{0.1}Nb_{0.1}O_{3-\delta}$	415	63	–	60 (Ar + H_2)	–	[68]
$Sr_{1.95}Fe_{1.4}Ni_{0.1}Mo_{0.5}O_{6-\delta}$	800	9	–	17 (pumped air 10^{-20} atm) 75 (wet H_2)	0.24 (600−800) –	[69]
$Sr_2Ni_{0.75}Mg_{0.25}MoO_6$	800	33.22	0.46 (400–800)	33 (pumped air 10^{-18} atm)	–	[73]
$PrBaMn_{1.5}Fe_{0.5}O_{5+\delta}$	800	112.2	–	7.4 (Ar + H_2)	–	[74]
$(La_{0.6}Sr_{0.4})_{0.9}Co_{0.2}Fe_{0.6}Nb_{0.2}O_{3-\delta}$	800	2.67	–	0.59	–	[75]
$La_{0.75}Sr_{0.25}Cr_{0.5}Mn_{0.5}O_{3-\delta}$	900	38	0.24 (300−900) 0.18 (20−300)	1.7 (Ar + H_2)	0.56 (300−900)	[76]

3.3. Electrochemical study

For an electrochemical device to operate efficiently, it is essential that electrode reactions, including the hydrogen oxidation reaction at the fuel electrode, occur at the highest possible rates. For this purpose, it is important that the electrodes exhibit high electrochemical activity. The electrochemical activity of the PSCFN electrodes in this study was examined in the symmetric cells with LSGM as the supporting electrolyte in a wet hydrogen atmosphere using impedance spectroscopy. Figure 3 illustrates the impedance spectra of the PSCFN electrode as an example. As can be observed, the spectra at 800 and 700 °C exhibit a relatively simple configuration, manifesting as a single half-circle. At 600 °C, the impedance spectrum clearly shows two half-circles. The DRT method was employed to analyze the spectra, which revealed that there was no significant shift in the frequency of the main peak, registered in the region of 10 Hz, within the temperature range of 600–800 °C. This suggests that the nature of the primary rate-determining stage of hydrogen oxidation at the PSCFN electrode remains unchanged across the entire temperature range. As observed in other strontium ferrite-based electrodes, the nature of this stage is likely associated with the low rate of dissociative adsorption of hydrogen on the electrode surface [22, 77].

The polarization resistances calculated from impedance spectra at different temperatures are shown in Figure 4. It can be seen that the temperature dependence in Arrhenius coordinates was linear. The calculated activation energy, determined from the slope of the dependence, was approximately 1 eV, which is consistent with the typical values observed for strontium ferrite-based electrodes in reducing atmospheres [22]. The obtained values of polarization resistance were high, reaching approximately $1 \, \Omega \cdot cm^2$ at 800 °C, which is suboptimal for an oxide fuel electrode (see Table 2).

One of the most effective and widespread methods of increasing electrochemical activity of electrodes is their impregnation with solutions of electroactive metals or oxides [78–80]. In the case of fuel electrodes, ceria has demonstrated efficacy in enhancing the activity of conventional nickel-based fuel electrodes by a factor of over tenfold [81, 82]. As illustrated in Figure 4, the introduction of ceria into the electrode allowed

Table 2 – Electrode performance in symmetrical cells with an LSGM electrolyte exposed in air or wet H_2.
("–" shows that there were no data available).

Electrode material	$R_{\eta_{air}}, \Omega \cdot cm^2$	$R_{\eta_{H_2}}, \Omega \cdot cm^2$	$T, °C$	Ref.
PSCFN	–	1.09	800	This study
		3.37	700	
CeO$_2$ infiltrated PSCFN	–	0.43	800	This study
		1.12	700	
Pr$_{0.4}$Sr$_{0.6}$Co$_{0.3}$Fe$_{0.6}$Nb$_{0.1}$O$_{3-\sigma}$	0.028	0.077	900	[54]
Pr$_{0.4}$Sr$_{0.6}$Co$_{0.19}$Fe$_{0.76}$Mo$_{0.05}$O$_{3-\sigma}$	0.06		700	[59]
Pr$_{0.8}$Sr$_{1.2}$(Co,Fe)$_{0.8}$Nb$_{0.2}$O$_{4+\delta}$ + Co-Fe alloy (Pr$_{0.4}$Sr$_{0.6}$Co$_{0.2}$Fe$_{0.7}$Nb$_{0.1}$O$_{3-\sigma}$ reduced in H$_2$ at 900 °C)	–	0.44	800	[52]
(Pr$_{0.4}$)$_{1.05}$Sr$_{0.6}$Co$_{0.2}$Fe$_{0.7}$Nb$_{0.1}$O$_{3-\sigma}$	0.012	0.135	900	[53]
		0.15	850	
		0.20	800	
Pr$_{0.4}$Sr$_{0.6}$Fe$_{0.875}$Mo$_{0.125}$O$_{3-\sigma}$	1.02	1.60	800	[70]
	1.79	2.78	750	
	2.99	5.30	700	
PrBaMn$_{1.5}$Fe$_{0.5}$O$_{5+\delta}$	0.22	0.68	800	[74]
Ba$_{0.95}$La$_{0.05}$Fe$_{0.9}$Nb$_{0.1}$O$_{3-\sigma}$	0.055	0.148	750	[71]
Ba$_{0.5}$Sr$_{0.5}$Mo$_{0.1}$Fe$_{0.9}$O$_{3-\sigma}$	0.007	0.047	800	[83]
Sr$_{1.95}$Fe$_{1.4}$Ni$_{0.1}$Mo$_{0.5}$O$_{6-\sigma}$	0.10	0.08	800	[69]
	0.42	0.12	700	
La$_{0.4}$Sr$_{0.6}$Co$_{0.2}$Fe$_{0.7}$Nb$_{0.1}$O$_{3-\sigma}$	0.075	0.22	850	[84]
	0.10		800	
	0.16		750	
(La$_{0.6}$Sr$_{0.4}$)$_{0.9}$Co$_{0.2}$Fe$_{0.6}$Nb$_{0.2}$O$_{3-\sigma}$	0.098	0.355	850	[75]
	0.164	0.382	800	
	0.300	0.464	700	

electrode activity, reaching the value of approximately 0.4 $\Omega \cdot cm^2$ at 800 °C, which is deemed satisfactory for practical applications. It is noteworthy that the incorporation of ceria into PSCFN did not result in a modification of the activation energy (Figure 4), which suggests that the underlying mechanism of the electrode reaction remained unaltered. This behavior is rather unusual, as in the case of nickel-ceramic fuel electrodes, the introduction of ceria into them dramatically changes both the activation energy of the polarization resistance and the kinetics of the electrode reaction [63]. To gain insight into this phenomenon, the impedance spectra and DRT function of PSCFN after impregnation were examined in detail.

Figure 5 shows the electrochemical impedance spectra of the PSCFN electrodes impregnated with ceria at different temperatures. A comparison of the data from Figure 3 and Figure 5 reveals that the introduction of ceria does not lead to a change in the impedance spectra shape. Furthermore, a comparison of the DRT functions for the original electrode and that after impregnation reveals that the appearance of the function did not change at all investigated temperatures. The characteristic relaxation frequencies of the maxima also remained unchanged. The introduction of ceria affected only the polarization resistance of the electrode (Figure 4). Given that ceria in a hydrogen atmosphere is partially reduced and becomes a mixed ion-electron conductor [85], it can be concluded that its introduction into PSCFN merely expands of the zone (area) of the electrochemical reaction of hydrogen oxidation without altering its mechanism.

To determine the stability of the electrochemical activity of PSCFN electrode impregnated with ceria, long-term tests were performed in a wet hydrogen at 800 °C for about 220 h. The time dependence of the polarization resistance is shown in Figure 6. As can be seen, the polarization resistance varies slightly during the investigated time. Small changes in the values have a random behavior without clear trends. Apparently, this can be attributed to the insignificant change in the partial pressure of water in the gas mixture. In general, the activity of the electrode remains almost unchanged. Attention should be drawn to the shift of the whole impedance spectrum to the lower impedance region with time (Figure 6), which is a non-typical behavior for electrochemical systems.

This behavior is most likely caused by changes in the electrode/electrolyte interface layer due to the formation of Co-Fe alloy (Figure 1), rather than in the electrode itself, since its activity remains almost unchanged. The stability of the electrode performance is also shown by the DRT functions calculated from the impedance spectra before and after long-term tests (Figure 6). It can be seen that
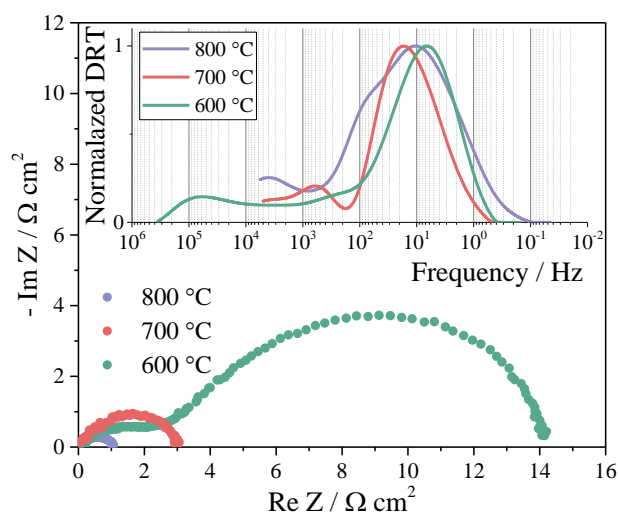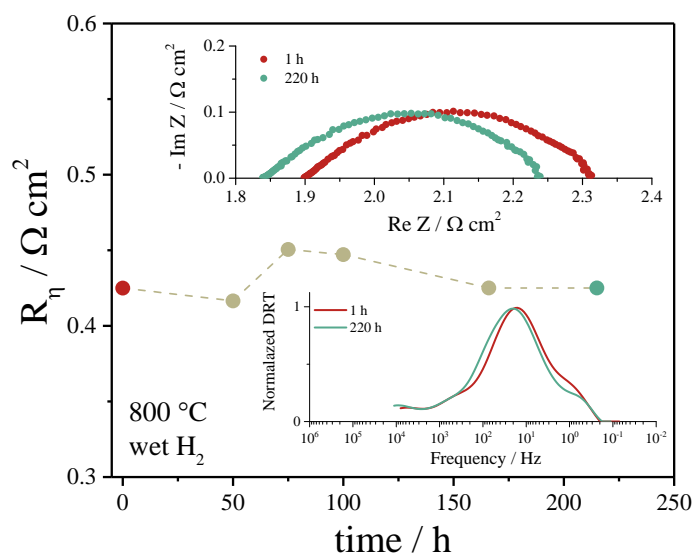

Figure 3 Impedance spectra and DRT functions for PSCFN electrode in wet hydrogen.
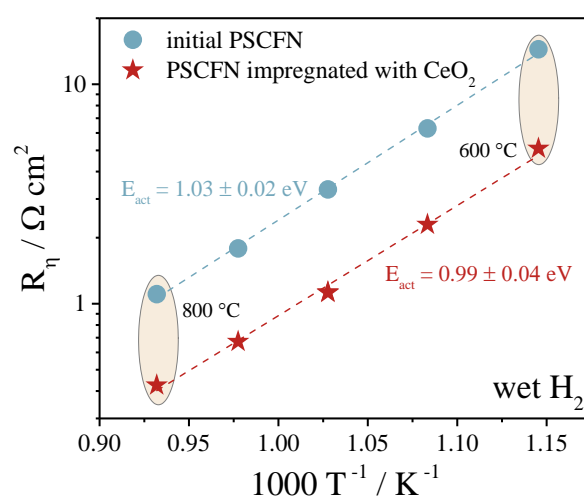
Figure 4 Polarization resistances of the PSCFN electrode before and after impregnation with ceria under wet hydrogen.
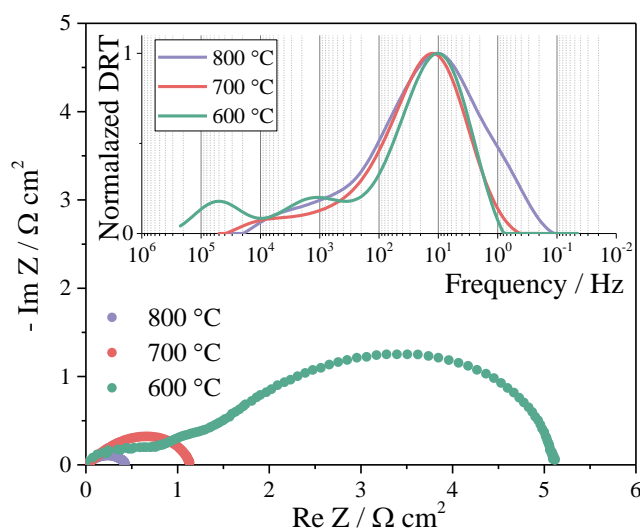
Figure 5 Impedance spectra and DRT functions for the PSCFN electrode impregnated with ceria in wet hydrogen.

Figure 6 Time dependences of the polarization resistance, impedance spectra and DRT function for the PSCFN electrode impregnated with ceria at 800 °C in a wet hydrogen.

the functions did not undergo any significant changes during the experiment, which indicates the stability of the electrode behavior over time.

4. Conclusion

This study presents the study of structural stability and features of electrical and electrochemical behavior of $Pr_{0.4}Sr_{0.6}Co_{0.2}Fe_{0.7}Nb_{0.1}O_{3-\delta}$ (PSCFN) material, potential for use in symmetrical solid oxide fuel cells, under reducing conditions. The PSCNF material, obtained via the solid-state reaction method in air with ta final sintering temperature increased up to 1150 °C, was single-phase and exhibited an orthorhombic structure. The oxide retained satisfactory structural stability at 800 °C in the atmosphere of 5 % H_2 + Ar. The electrical conductivity of PSCFN in wet hydrogen exhibited a linear semiconductor-type behavior with a conductivity value of 7 S · cm⁻¹ at 800 °C with an activation energy of 0.24 eV, close to those reported in the literature for similar materials. The polarization resistance of the electrode in wet hydrogen atmosphere was 1.09 and 3.37 $\Omega \cdot cm^2$ at 800 and 700 °C, respectively, which is quite high for the electrodes of electrochemical devices. The introduction of ceria into the electrode allowed approximately threefold enhancement in the PSCFN electrode activity, reaching the value of approximately 0.43 and 1.12 $\Omega \cdot cm^2$ at 800 and 700 °C, respectively. A comprehensive DRT analysis of the spectra obtained demonstrated that the observed decrease in the polarization resistance occurred without changing the mechanism of hydrogen oxidation and was merely due to the expansion of the area of the electrochemical reaction. The activated PSCFN electrode

demonstrated satisfactory stability of the electrochemical activity being tested during 220 h at 800 °C in a wet hydrogen atmosphere. Summarizing, the findings of this study revealed that PSCFN material obtained at an increased synthesis temperature demonstrates enhanced stability in hydrogen. When utilized as an electrode, it requires activation to demonstrate electrochemical activity that is satisfactory of the LSGM-based electrochemical devices operating in the intermediate temperature range.

Supplementary materials

No supplementary materials are available.

Funding

Acknowledgments

Author contributions

Elena Pikalova: Conceptualization; Data curation; Formal Analysis; Writing – Original draft, Writing – Review & Editing.

Denis Osinkin: Investigation; Data curation; Methodology; Supervision. Writing – Original draft.

Conflict of interest

The authors declare no conflict of interest' or declare any potential (ethical, financial) interests if they exist.

Additional information

Elena Pikalova, Scopus Author ID: 16242376500;
Denis Osinkin, Scopus Author ID: 26536496100.

References

1. Singh M, Zappa D, Comini E, Solid oxide fuel cell: Decade of progress, future perspectives and challenges, Int. J. Hydrog. Energy, **46(54)** (2021) 27643–27674. https://doi.org/10.1016/j.ijhydene.2021.06.020

2. Demin AK, Bronin DI, Solid state electrochemical devices for hydrogen energy, Electrochem. Mater. Technol., **2** (2023) 20232016. https://doi.org/10.15826/elmattech.2023.2.016

3. Jiang S, Advances and Challenges of Intermediate Temperature Solid Oxide Fuel Cells: A Concise Review, J. Electrochem., **18(6)** (2012) 1. https://doi.org/10.61558/2993-074X.2617

4. Sadykov VA, Eremeev NF, Sadovskaya EM, et al., Design of materials for solid oxide fuel cells, permselective membranes, and catalysts for biofuel transformation into

syngas and hydrogen based on fundamental studies of their real structure, transport properties, and surface reactivity, Curr. Opin. Green Sustain. Chem., **33** (2022) 100558. https://doi.org/10.1016/j.cogsc.2021.100558

5. Mah JCW, Muchtar A, Somalu MR, Ghazali MJ, Metallic interconnects for solid oxide fuel cell: A review on protective coating and deposition techniques, Int. J. Hydrog. Energy., **42(14)** (2017) 9219–9229. https://doi.org/10.1016/j.ijhydene.2016.03.195

6. Sharifzadeh M, Chen W, Triulzi G, et al., Design and operation of solid oxide fuel cell systems: challenges and future research directions. In: Design and Operation of Solid Oxide Fuel Cells. Elsevier; 2020. pp 445–463.

7. Zhu Q, Peng L, Zhang T, Stable Glass Seals for Intermediate Temperature (IT) SOFC Applications. In: Kuang K, Easler K (eds) Fuel Cell Electronics Packaging. Springer US, Boston, MA; 2007. pp 33–60.

8. Mendonça C, Ferreira A, Santos DMF, Towards the Commercialization of Solid Oxide Fuel Cells: Recent Advances in Materials and Integration Strategies, Fuels, **2(4)** (2021) 393–419. https://doi.org/10.3390/fuels2040023

9. Dwivedi S, Solid oxide fuel cell: Materials for anode, cathode and electrolyte, Int. J. Hydrog. Energy, **45(44)** (2020) 23988–24013. https://doi.org/10.1016/j.ijhydene.2019.11.234

10. Istomin SY, Antipov EV, Cathode materials based on perovskite-like transition metal oxides for intermediate temperature solid oxide fuel cells, Russ. Chem. Rev., **82** (2013) 686–700. https://doi.org/10.1070/RC2013v082n07ABEH004390

11. Xu H, Han Y, Zhu J, et al., Status and progress of metal-supported solid oxide fuel cell: Towards large-scale manufactory and practical applications, Energy Rev., **3(1)** (2024) 100051. https://doi.org/10.1016/j.enrev.2023.100051

12. Pikalova EYu, Kalinina EG, Place of electrophoretic deposition among thin-film methods adapted to the solid oxide fuel cell technology: A short review, Int. J. Energy Prod. Manag., **4(1)** (2019) 1–27. https://doi.org/10.2495/EQ-V4-N1-1-27

13. Dunyushkina LA, Solid Oxide Fuel Cells with a Thin Film Electrolyte: A Review on Manufacturing Technologies and Electrochemical Characteristics, Electrochem. Mater. Technol., **1** (2022) 20221006. https://doi.org/10.15826/elmattech.2022.1.006

14. Pikalova EYu, Kalinina EG, Solid oxide fuel cells based on ceramic membranes with mixed conductivity: improving efficiency, Russ. Chem. Rev., **90** (2021) 703–749. https://doi.org/10.1070/RCR4966

15. Antonova EP, Proton-conducting oxides based on $LaScO_3$: structure, properties and electrochemical applications. A focus review, Electrochem. Mater. Technol., **2** (2023) 20232021. https://doi.org/10.15826/elmattech.2023.2.021

16. Filonova E, Medvedev D, Recent Progress in the Design, Characterisation and Application of $LaAlO_3$- and $LaGaO_3$-Based Solid Oxide Fuel Cell Electrolytes, Nanomaterials, **12** (2022) 1991. https://doi.org/10.3390/nano12121991

17. Tahir NNM, Baharuddin NA, Samat AA, Osman N, Somalu MR, A review on cathode materials for conventional and proton-conducting solid oxide fuel cells, J. Alloys Compd., **894** (2022) 162458. https://doi.org/10.1016/j.jallcom.2021.162458

18. Kaur P, Singh K, Review of perovskite-structure related cathode materials for solid oxide fuel cells, Ceram. Int., **46(5)** (2020) 5521–5535. https://doi.org/10.1016/j.ceramint.2019.11.066

19. Baratov S, Filonova E, Ivanova A, et al., Current and further trajectories in designing functional materials for solid oxide electrochemical cells: A review of other reviews, J. Energy Chem., **94** (2024) 302–331. https://doi.org/10.1016/j.jechem.2024.02.047

20. Yáng Z, Martynczuk J, Efimov K, et al., Oxygen-Vacancy-Related Structural Phase Transition of $Ba_{0.8}Sr_{0.2}Co_{0.8}Fe_{0.2}O_{3-\delta}$, Chem. Mater., **23** (2011) 3169–3175. https://doi.org/10.1021/cm200373r

21. Pan Z, Liu Q, Zhang L, et al., Effect of Sr Surface Segregation of $La_{0.6}Sr_{0.4}Co_{0.2}Fe_{0.8}O_{3-\delta}$ Electrode on Its Electrochemical Performance in SOC, J. Electrochem. Soc., **162** (2015) F1316–F1323. https://doi.org/10.1149/2.0371512jes

22. Koo B, Kim K, Kim JK, et al., Sr Segregation in Perovskite Oxides: Why It Happens and How It Exists, Joule, **2(8)** (2018) 1476–1499. https://doi.org/10.1016/j.joule.2018.07.016

23. Safian SD, Abd Malek NI, Jamil Z, et al., Study on the surface segregation of mixed ionic-electronic conductor lanthanum-based perovskite oxide $La_{1-x}Sr_xCo_{1-y}Fe_yO_{3-\delta}$ materials, Int. J. Energy Res., **46** (2022) 7101–7117. https://doi.org/10.1002/er.7733

24. Shah N, Xu X, Love J, et al., Mitigating thermal expansion effects in solid oxide fuel cell cathodes: A critical review, J. Power Sources, **599** (2024) 234211. https://doi.org/10.1016/j.jpowsour.2024.234211

25. Lyagaeva J, Medvedev D, Pikalova E, et al., A detailed analysis of thermal and chemical compatibility of cathode materials suitable for $BaCe_{0.8}Y_{0.2}O_{3-\delta}$ and $BaZr_{0.8}Y_{0.2}O_{3-\delta}$ proton electrolytes for solid oxide fuel cell application, Int. J. Hydrog. Energy, **42(3)** (2024) 1715–1723. https://doi.org/10.1016/j.ijhydene.2016.07.248

26. Pikalova EYu, Guseva EM, Filonova EA, Short review on recent studies and prospects of application of rare-earth-doped $La_2NiO_{4+\delta}$ as air electrodes for solid-oxide electrochemical cells, Electrochem. Mater. Technol., **2** (2023) 20232025. https://doi.org/10.15826/elmattech.2023.2.025

27. Ndubuisi A, Abouali S, Singh K, Thangadurai V, Recent advances, practical challenges, and perspectives of intermediate temperature solid oxide fuel cell cathodes, J. Mater. Chem. A, **10** (2022) 2196–2227. https://doi.org/10.1039/D1TA08475E

28. Ahmad MZ, Ahmad SH, Chen RS, et al., Review on recent advancement in cathode material for lower and intermediate temperature solid oxide fuel cells application, Int. J. Hydrog. Energy, **47(2)** (2022) 1103–1120. https://doi.org/10.1016/j.ijhydene.2021.10.094

29. Sadykov V, Pikalova E, Sadovskaya E, et al., Design of Mixed Ionic-Electronic Materials for Permselective Membranes and Solid Oxide Fuel Cells Based on Their Oxygen and Hydrogen Mobility, Membranes, **13(8)** (2023) 698. https://doi.org/10.3390/membranes13080698

30. Shaikh SPS, Muchtar A, Somalu MR, A review on the selection of anode materials for solid-oxide fuel cells, Renew. Sustain. Energy Rev., **51** (2015) 1–8. https://doi.org/10.1016/j.rser.2015.05.069

31. Ahmed N, Devi S, Dar MA, et al., Anode material for solid oxide fuel cell: a review, Indian J. Phys., **98** (2024) 877–888. https://doi.org/10.1007/s12648-023-02860-3

32. Zainon AN, Somalu MR, Kamarul Bahrain AM, et al., Challenges in using perovskite-based anode materials for solid oxide fuel cells with various fuels: a review, Int. J. Hydrog. Energy, **48(53)** (2023) 20441–20464. https://doi.org/10.1016/j.ijhydene.2022.12.192

33. Shu L, Sunarso J, Hashim SS, et al., Advanced perovskite anodes for solid oxide fuel cells: A review, Int. J. Hydrog. Energy, **44(59)** (2019) 31275–31304. https://doi.org/10.1016/j.ijhydene.2019.09.220

34. Osinkin DA, Some aspects of hydrogen oxidation in solid oxide fuel cell: A brief historical overview, Electrochem. Mater. Technol., **2** (2023) 20232018. https://doi.org/10.15826/elmattech.2023.2.018

35. Khrustov AV, Ananyev MV, Bronin DI, et al., Characterisation of Ni-cermet degradation phenomena II. Relationship between connectivity and resistivity, J. Power Sources, **497** (2021) 229847. https://doi.org/10.1016/j.jpowsour.2021.229847

36. Chen H, Wang F, Wang W, et al., H_2S poisoning effect and ways to improve sulfur tolerance of nickel cermet anodes operating on carbonaceous fuels, Appl. Energy, **179** (2016) 765–777. https://doi.org/10.1016/j.apenergy.2016.07.028

37. Istomin SYa, Lyskov NV, Mazo GN, Antipov EV, Electrode materials based on complex d-metal oxides for symmetrical solid oxide fuel cells, Russ. Chem. Rev., **90** (2021) 644–676. https://doi.org/10.1070/RCR4979

38. Yusoff WNAW, Baharuddin NA, Somalu MR, et al., A Short Review on Selection of Electrodes Materials for Symmetrical Solid Oxide Fuel Cell, IOP Conf. Series: Mater. Sci. Engin., **957** (2020) 012049. https://doi.org/10.1088/1757-899X/957/1/012049

39. Arregui A, Rodriguez-Martinez LM, Modena S, et al., Stability of ferritic perovskite cathodes in anode-supported solid oxide fuel cells under different processing and operation parameters, Electrochim. Acta, **58** (2011) 312–321. https://doi.org/10.1016/j.electacta.2011.09.048

40. Xu X, Su C, Shao Z, Fundamental Understanding and Application of $Ba_{0.5}Sr_{0.5}Co_{0.8}Fe_{0.2}O_{3-\delta}$ Perovskite in Energy Storage and Conversion: Past, Present, and Future, Energy Fuels, **35(17)** (2021) 13585–13609. https://doi.org/10.1021/acs.energyfuels.1c02111

41. Fernández-Ropero AJ, Porras-Vázquez JM, Cabeza A, et al., High valence transition metal doped strontium ferrites for electrode materials in symmetrical SOFCs, J. Power Sources, **249** (2014) 405–413. https://doi.org/10.1016/j.jpowsour.2013.10.118

42. Liu F, Zhang L, Huang G, et al., High performance ferrite–based anode $La_{0.5}Sr_{0.5}Fe_{0.9}Mo_{0.1}O_{3-\delta}$ for intermediate–temperature solid oxide fuel cell, Electrochim. Acta, **255** (2017) 118–126. https://doi.org/10.1016/j.electacta.2017.09.157

43. Yang X, Li R, Yang Y, et al., Improving stability and electrochemical performance of $Ba_{0.5}Sr_{0.5}Co_{0.2}Fe_{0.8}O_{3-\delta}$ electrode for symmetrical solid oxide fuel cells by Mo doping, J. Alloys Compd., **831** (2020) 154711. https://doi.org/10.1016/j.jallcom.2020.154711

44. Teketel BS, Beshiwork BA, Desta HG, et al., Ta/Nb doping motivating cubic phase stability and CO_2 tolerance of $Sr_2Co_{1.6}Fe_{0.4}O_{6-\delta}$ double perovskite for high-performing SOFC cathode, Ceram. Int., **50(7A)** (2024) 11246–11258. https://doi.org/10.1016/j.ceramint.2024.01.025

45. Li D, Zhang X, Jin Y, et al., Suppression of Sr surface segregation in $La_{0.8}Sr_{0.2}Co_{0.2}Fe_{0.8}O_{3-\delta}$ via Nb doping in B-site, Ceram. Int., **48(2)** (2022) 2161–2168. https://doi.org/10.1016/j.ceramint.2021.09.305

46. Chivite-Lacaba M, Prado-Gonjal J, Alonso JA, et al., High performance of $SrCo_{1-x}Zr_xO_{3-\delta}$ perovskite cathodes for IT-SOFCs, Ceram. Int., **50(15)** (2024) 26929–26937. https://doi.org/10.1016/j.ceramint.2024.04.424

47. Zamudio-García J, Caizán-Juanarena L, Porras-Vázquez JM, et al., A review on recent advances and trends in symmetrical electrodes for solid oxide cells, J. Power Sources, **520** (2022) 230852. https://doi.org/10.1016/j.jpowsour.2021.230852

48. Meng X, Lü S, Ji Y, et al., Characterization of $Pr_{1-x}Sr_xCo_{0.8}Fe_{0.2}O_{3-\delta}$ ($0.2 \leq x \leq 0.6$) cathode materials for intermediate-temperature solid oxide fuel cells, J. Power Sources, **183(2)** (2008) 581–585. https://doi.org/10.1016/j.jpowsour.2008.05.052

49. Patro PK, Delahaye T, Bouyer E, Development of $Pr_{0.58}Sr_{0.4}Fe_{0.8}Co_{0.2}O_{3-\delta}$-GDC composite cathode for solid oxide fuel cell (SOFC) application, Solid State Ion., **181(29–30)** (2010) 1378–1386. https://doi.org/10.1016/j.ssi.2010.07.004

50. Liu X, Li M, Wang Z, et al., Electro-spinning $Pr_{0.4}Sr_{0.6}Co_{0.2}Fe_{0.7}Nb_{0.1}O_{3-\delta}$ nanofibers infiltrated with $Gd_{0.2}Ce_{0.8}O_{1.9}$ nanoparticles as cathode for intermediate temperature solid oxide fuel cell, Ceram. Int., **42(10)** (2016) 11907–11912. https://doi.org/10.1016/j.ceramint.2016.04.113

51. Kim JH, Baek S-W, Lee C, et al., Performance analysis of cobalt-based cathode materials for solid oxide fuel cell, Solid State Ion., **179(27–32)** (2008) 1490–1496. https://doi.org/10.1016/j.ssi.2008.01.086

52. Yang C, Yang Z, Jin C, et al., Sulfur-Tolerant Redox-Reversible Anode Material for Direct Hydrocarbon Solid Oxide Fuel Cells, Adv. Mater., **24(11)** (2012) 1439–1443. https://doi.org/10.1002/adma.201104852

53. Zhang P, Guan G, Khaerudini DS, et al., Properties of A-site nonstoichiometry $(Pr_{0.4})Sr_{0.6}Co_{0.2}Fe_{0.7}Nb_{0.1}O_{3-\delta}$ ($0.9 \leq x \leq 1.1$) as symmetrical electrode material for solid oxide fuel cells, J. Power Sources, **248** (2014) 163–171. https://doi.org/10.1016/j.jpowsour.2013.09.077

54. Xiaokaiti P, Yu T, Yoshida A, et al., Effects of cobalt and iron proportions in $Pr_{0.4}Sr_{0.6}Co_{0.9-x}Fe_xNb_{0.1}O_{3-\delta}$ electrode material for symmetric solid oxide fuel cells, J. Alloys Compd., **831** (2020) 154738. https://doi.org/10.1016/j.jallcom.2020.154738

55. Li P, Dong R, Wang Y, et al., Improving the performance of $Pr_{0.4}Sr_{0.6}Co_{0.2}Fe_{0.7}Nb_{0.1}O_{3-\delta}$-based single-component fuel cell and reversible single-component cells by manufacturing A-site deficiency, Renew. Energy, **177** (2021) 387–396. https://doi.org/10.1016/j.renene.2021.05.141

56. Partovi K, Geppert B, Liang F, et al., Effect of the B-Site Composition on the Oxygen Permeability and the CO_2 Stability of $Pr_{0.6}Sr_{0.4}Co_xFe_{1-x}O_{3-\delta}$ ($0.0 \leq x \leq 1.0$) Membranes, Chem. Mater., **27(8)** (2015) 2911–2919. https://doi.org/10.1021/acs.chemmater.5b00166

57. Zhao Z, Rehder L, Steinbach F, Feldhoff A, High-Entropy Perovskites $Pr_{1-x}Sr_x(Cr,Mn,Fe,Co,Ni)O_{3-\delta}$ ($x=0$–0.5): Synthesis and Oxygen Permeation Properties, Membranes, **12(11)** (2022) 1123. https://doi.org/10.3390/membranes12111123

58. Ishihara T, Kudo T, Matsuda H, Takita Y, Doped PrMnO$_3$ Perovskite Oxide as a New Cathode of Solid Oxide Fuel Cells for Low Temperature Operation, J. Electrochem. Soc., 142(5) (1995) 1519–1524. https://doi.org/10.1149/1.2048606

59. Zhang P, Guan G, Khaerudini DS, et al., Mo doped Pr$_{0.4}$Sr$_{0.6}$Co$_{0.2}$Fe$_{0.8}$O$_{3-\delta}$ cathode material with high catalytic activity for intermediate-temperature solid oxide fuel cells, Electrochim. Acta, 146 (2014) 591–597. https://doi.org/10.1016/j.electacta.2014.08.154

60. Gordeev EV, Porotnikova NM, Approaches for the preparation of dense ceramics and sintering aids for Sr/Mg doped lanthanum gallate: focus review, Electrochem. Mater. Technol., 2 (2023) 20232022. https://doi.org/10.15826/elmattech.2023.2.022

61. Gorelov VP, Bronin DI, Sokolova JuV, et al., The effect of doping and processing conditions on properties of La$_{1-x}$Sr$_x$Ga$_{1-y}$Mg$_y$O$_{3-\alpha}$, J. Eur. Ceram. Soc., 21(13) (2001) 2311–2317. https://doi.org/10.1016/S0955-2219(01)00203-5

62. Osinkin DA, Complementary effect of ceria on the hydrogen oxidation kinetics on Ni-Ce$_{0.8}$Sm$_{0.2}$O$_{2-\delta}$ anode, Electrochim. Acta, 330 (2020) 135257. https://doi.org/10.1016/j.electacta.2019.135257

63. Osinkin DA, An approach to the analysis of the impedance spectra of solid oxide fuel cell using the DRT technique, Electrochim. Acta, 372 (2021) 137858. https://doi.org/10.1016/j.electacta.2021.137858

64. Xiaokaiti P, Yu T, Yoshida A, et al., Characterization of B-Site Niobium-Doped Pr$_{0.4}$Sr$_{0.6}$(Co$_{0.3}$Fe$_{0.6}$)$_{1-x}$Nb$_x$O$_{3-\delta}$ (x=0, 0.05, 0.1, 0.2) Perovskites as Cathode Materials for Solid Oxide Fuel Cells, ChemistrySelect, 3(17) (2018) 4609–4618. https://doi.org/10.1002/slct.201702180

65. Patrakeev MV, Mitberg EB, Lakhtin AA, et al., Oxygen Nonstoichiometry, Conductivity, and Seebeck Coefficient of La$_{0.3}$Sr$_{0.7}$Fe$_{1-x}$Ga$_x$O$_{2.65+\delta}$ Perovskites, J. Solid State Chem., 167(1) (2002) 203–213. https://doi.org/10.1006/jssc.2002.9644

66. Rietveld HM, A profile refinement method for nuclear and magnetic structures, J. Appl. Crystallogr., 2 (1969) 65–71. https://doi.org/10.1107/S0021889869006558

67. Zhang P, Guan G, Khaerudini DS, et al., B-site Mo-doped perovskite Pr$_{0.4}$Sr$_{0.6}$(Co$_{0.2}$Fe$_{0.8}$)$_{1-x}$Mo$_x$O$_{3-\delta}$ (x = 0, 0.05, 0.1 and 0.2) as electrode for symmetrical solid oxide fuel cell. J. Power Sources, 276 (2015) 347–356. https://doi.org/10.1016/j.jpowsour.2014.11.141

68. Lan R, Cowin PI, Sengodan S, Tao S, A perovskite oxide with high conductivities in both air and reducing atmosphere for use as electrode for solid oxide fuel cells, Sci. Rep., 6 (2016) 31839. https://doi.org/10.1038/srep31839

69. Osinkin DA, Antonova EP, Shubin KS, Bogdanovich NM, Influence of nickel exsolution on the electrochemical performance and rate-determining stages of hydrogen oxidation on Sr$_{1.95}$Fe$_{1.4}$Ni$_{0.1}$Mo$_{0.5}$O$_{6-\delta}$ promising electrode for solid state electrochemical devices, Electrochim. Acta, 369 (2021) 137673. https://doi.org/10.1016/j.electacta.2020.137673

70. Zhang D, Zhang K, He T, et al., Preparation and characterization of a redox-stable Pr$_{0.4}$Sr$_{0.6}$Fe$_{0.875}$Mo$_{0.125}$O$_{3-\delta}$ material as a novel symmetrical electrode for solid oxide cell application, Int. J. Hydrog. Energy, 45(41) (2020) 21825–21835. https://doi.org/10.1016/j.ijhydene.2020.05.206

71. Li Z, Wang J, Zhu J, et al., A novel Ba$_{0.95}$La$_{0.05}$Fe$_{0.9}$Nb$_{0.1}$O$_{3-\delta}$ ceramic electrode for symmetrical solid oxide fuel cells. Sustain, Energy Fuels, 5 (2021) 5975–5984. https://doi.org/10.1039/D1SE01291F

72. Wu Y, Yang Y, Zhou S, et al., Enhanced redox-stable Sm$_{0.5}$Sr$_{0.5}$FeO$_{3-\delta}$ electrode material for symmetric solid oxide fuel cells at reduced temperatures, Ceram. Int., 46(5) (2020) 6714–6722. https://doi.org/10.1016/j.ceramint.2019.11.160

73. Filonova EA, Dmitriev AS, Pikalov PS, et al., The structural and electrical properties of Sr$_2$Ni$_{0.75}$Mg$_{0.25}$MoO$_6$ and its compatibility with solid state electrolytes, Solid State Ion., 262 (2014) 365–369. https://doi.org/10.1016/j.ssi.2013.11.036

74. Zhao L, Chen K, Liu Y, He B, A novel layered perovskite as symmetric electrode for direct hydrocarbon solid oxide fuel cells, J. Power Sources, 342 (2017) 313–319. https://doi.org/10.1016/j.jpowsour.2016.12.066

75. Niu B, Jin F, Feng T, et al., A-site deficient (La$_{0.6}$Sr$_{0.4}$)$_{1-x}$Co$_{0.2}$Fe$_{0.6}$Nb$_{0.2}$O$_{3-\delta}$ symmetrical electrode materials for solid oxide fuel cells, Electrochim. Acta, 270 (2018) 174–182. https://doi.org/10.1016/j.electacta.2018.03.085

76. Tao S, Irvine JTS, A redox-stable efficient anode for solid-oxide fuel cells, Nat. Mater., 2 (2003) 320–323. https://doi.org/10.1038/nmat871

77. Osinkin DA, Hydrogen oxidation kinetics on a redox stable electrode for reversible solid-state electrochemical devices: The critical influence of hydrogen dissociation on the electrode surface, Electrochim. Acta, 389 (2021) 138792. https://doi.org/10.1016/j.electacta.2021.138792

78. Jiang SP, A review of wet impregnation—An alternative method for the fabrication of high performance and nano-structured electrodes of solid oxide fuel cells, Mater. Sci. Eng. A, 418(1–2) (2006) 199–210. https://doi.org/10.1016/j.msea.2005.11.052

79. Ding D, Li X, Lai SY, et al., Enhancing SOFC cathode performance by surface modification through infiltration, Energy Environ. Sci., 7 (2014) 552. https://doi.org/10.1039/c3ee42926a

80. Filonova E, Pikalova E, Overview of Approaches to Increase the Electrochemical Activity of Conventional Perovskite Air Electrodes, Materials, 16(14) (2023) 4967. https://doi.org/10.3390/ma16144967

81. Osinkin DA, Bogdanovich NM, Gavrilyuk AL, Rate determining steps of fuel oxidation over CeO$_2$ impregnated Ni-YSZ in H$_2$+H$_2$O+CO+CO$_2$ ambient, Electrochim. Acta, 199 (2016) 108–115. https://doi.org/10.1016/j.electacta.2016.03.133

82. Osinkin DA, Bogdanovich NM, Beresnev SM, Zhuravlev VD, High-performance anode-supported solid oxide fuel cell with impregnated electrodes, J. Power Sources, 288 (2015) 20–25. https://doi.org/10.1016/j.jpowsour.2015.04.098

83. Yang Z, Wang W, Xiao J, et al., A novel cobalt-free Ba$_{0.5}$Sr$_{0.5}$Fe$_{0.9}$Mo$_{0.1}$O$_{3-\delta}$–BaZr$_{0.1}$Ce$_{0.7}$Y$_{0.2}$O$_{3-\alpha}$ composite cathode for solid oxide fuel cells, J. Power Sources, 204 (2012) 89–93. https://doi.org/10.1016/j.jpowsour.2012.01.044

84. Yang Z, Xu N, Han M, Chen F, Performance evaluation of La$_{0.4}$Sr$_{0.6}$Co$_{0.2}$Fe$_{0.7}$Nb$_{0.1}$O$_{3-\delta}$ as both anode and cathode material in solid oxide fuel cells, Int. J. Hydrog. Energy, 39(14) (2014) 7402–7406. https://doi.org/10.1016/j.ijhydene.2014.01.009

85. Pikalova EYu, Maragou VI, Demina AN, et al., The effect of co-dopant addition on the properties of Ln$_{0.2}$Ce$_{0.8}$O$_{2-\delta}$ (Ln=Gd, Sm, La) solid-state electrolyte, J. Power Sources, 181(2) (2008) 199–206. https://doi.org/10.1016/j.jpowsour.2008.02.003